F. FALO[1],✉
P.J. MARTÍNEZ[2]
J.J. MAZO[1]
T.P. ORLANDO[3]
K. SEGALL[3]
E. TRÍAS[3]

Fluxon ratchet potentials in superconducting circuits

[1] Departamento de Física de la Materia Condensada and ICMA, CSIC-Universidad de Zaragoza, 50009 Zaragoza, Spain
[2] Departamento de Física Aplicada and ICMA, CSIC-Universidad de Zaragoza, 50009 Zaragoza, Spain
[3] Department of Electrical Engineering and Computer Science, Massachusetts Institute of Technology, Cambridge, MA 02139, USA

ABSTRACT A fluxon in a Josephson-junction parallel array behaves like a single particle in a periodic pinning potential. Different configurations of critical currents and cell areas result in different profiles for the fluxon potential. We analyze the minimal conditions to achieve an effective potential in which mirror symmetry is absent, namely a fluxon ratchet potential. Following one of the configurations, we designed circular arrays and probed some of the fluxon properties. Theoretical predictions are nicely fulfilled by the experiments.

PACS 05.40-a; 74.50+r; 85.25Na

1 Introduction

Directional motion of particles [1] is an active field of research which is rapidly moving from basic to applied physics. Although initial attempts have been made to apply the underlying ideas to biomolecular motors [2, 3], the most promising applications belong to the world of nano- and micro-technologies. At a molecular level some interesting designs have been proposed [4], but it seems that an easier experimental realization could be achieved at the micrometer scale. Towards this aim, devices based on the Josephson effect are being proposed and studied. Zapata et al. [5] have proposed a ratchet SQUID with one and two junctions respectively in each arm to break the spatial symmetry. Following this idea other designs have been cast using the effective potential created by an external magnetic field in a long Josephson junction [6, 7]. In superconducting thin films several mechanisms and applications have been proposed related to directional vortex (or flux) motion. Lee et al. [8] devised a method for "cleaning" parasitic vortices from superconducting devices using an appropriate geometric ratchet potential. Fluxons also can be "directed" and "focused" using ratchet effective potentials [9].

We study the properties of a fluxon in parallel Josephson-junction (JJ) arrays. JJ arrays are becoming an excellent workbench for the predictions of non-linear dynamics theory. In particular, parallel arrays are experimental realizations of the Frenkel–Kontorova (FK) or discrete sine-Gordon (sG) model [10]. A fluxon in the Josephson array behaves like a kink in this system. The feasibility of fabricating microelectronic circuits with any desired geometry and a broad range of physical parameters allows one to obtain any energy profile for the fluxon. In this review, we first describe the physics and equations for fluxons in an inhomogeneous array. We calculate the dynamical properties of a fluxon for different parameters of the array, showing that, in some general circumstances, it exhibits a ratchet behavior [11]. Finally it is shown how the experiments in fabricated microcircuits fulfill the predicted critical current and external field dependence [12].

2 Parallel array

A JJ is a solid-state device that consists of two superconductors which are linked by a non-superconducting region [13]. The main physical properties of the junction are given by the Josephson relations:

$$V = \frac{\Phi_0}{2\pi}\dot{\varphi}, \quad I = I_c \sin \varphi, \tag{1}$$

where φ stands for the superconducting phase difference between both sides of the junction and V and I are the voltage and the current across the junction respectively. The critical current, I_c, is the maximum superconducting current the junction can support, and $\Phi_0 = h/2e$ is the flux quantum.

Using lithographic techniques is possible to construct arrays of well-characterized JJs. In one dimension, series arrays have been mainly studied in the context of synchronization of harmonic oscillators [14]. On the other hand, one-dimensional parallel arrays have been studied as a system for fluxon transport [15].

Here, we consider circular arrays formed by JJs connected in parallel (see Fig. 1). We will consider junctions shunted by small resistors (R_s); thus capacitive effects can be neglected, and we are in the overdamped limit of the array. We derive the basic equations of this system:

$$\frac{V_j}{R_s} + I_{cj} \sin \varphi_j = I(t) + I_{j-1} - I_j. \tag{2}$$

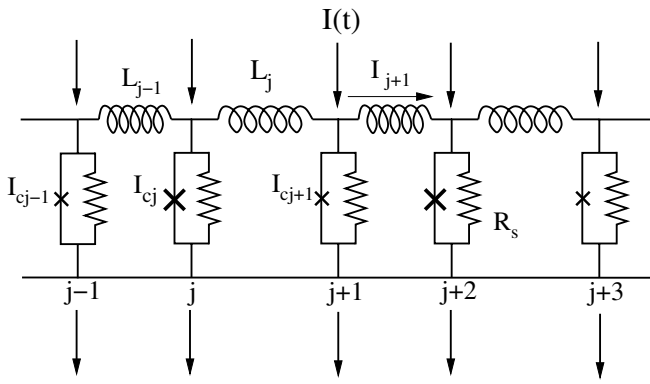✉ Fax: +34-976/76-1229, E-mail: fff@posta.unizar.es

FIGURE 1 Equivalent circuit of the parallel Josephson-junction (JJ) array. Each JJ is shunted by a resistance in order to have overdamped dynamics. L_j represents the plaquette self-inductance

The phase difference around a plaquette is given by

$$\varphi_{j+1} - \varphi_j = 2\pi \frac{\Phi_j}{\Phi_0} \,, \tag{3}$$

where

$$\Phi_j = \Phi^{\text{ext}} - L_j I_j \tag{4}$$

is the magnetic flux through a plaquette – the sum of two contributions: external and induced magnetic fields – where L is the total self-inductance of the cell.[1] In this paper we will set $\Phi^{\text{ext}} = 0$.

Combining (1), (2), (3) and (4), we obtain

$$\frac{\Phi_0}{2\pi R_s} \dot{\varphi}_j + I_{cj} \sin \varphi_j = I(t) + \frac{\Phi_0}{2\pi L_{j-1}} (\varphi_{j-1} - \varphi_j)$$
$$+ \frac{\Phi_0}{2\pi L_j} (\varphi_{j+1} - \varphi_j) \,, \tag{5}$$

and by normalizing the current by one of the critical currents, I_c, and time by $2\pi R_s I_c / \Phi_0$, we obtain the dimensionless equations

$$\dot{\varphi}_j + h_j \sin \varphi_j = \frac{I(\tau)}{I_c} + \lambda_{j-1}(\varphi_{j-1} - \varphi_j)$$
$$+ \lambda_j (\varphi_{j+1} - \varphi_j) \,, \tag{6}$$

where $h_j = I_{cj}/I_c$ and $\lambda_j = \Phi_0/2\pi I_c L_j$. We have to impose periodic boundary conditions: $\varphi_{j+N} = \varphi_j + 2\pi M$, where N is the number of junctions and M is the number of topological excitations (discrete solitons or kinks) in the circular array.

For uniform arrays the self-inductances, L, and critical currents, I_c, are independent of index j. Then, the equations correspond to the well-known standard FK model, whose static and dynamical properties have been intensively studied over the last few years [10, 16, 17]. This model was initially proposed as a model for the study of dislocations but has become paradigmatic for the study of modulated phases, dynamical phase transitions and kink dynamics. The FK model can be visualized as a model for a set of non-linear pendula coupled by harmonic springs. Its continuous limit [$(\varphi_{j+1} -$
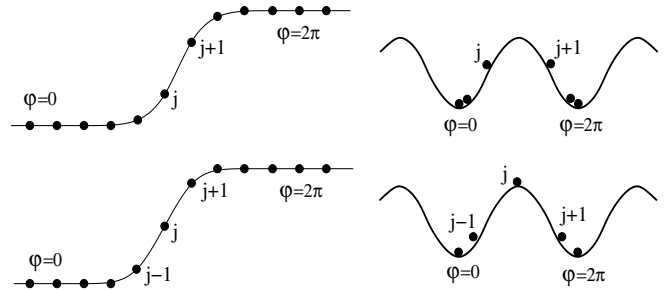

FIGURE 2 Schematic of a fluxon (discrete soliton or kink) in the parallel array. *Upper panel*: fluxon minimum configuration. *Lower panel*: saddle-point configuration. Energy differences between them define the Peierls–Nabarro barrier

$\varphi_j) \to 0$ and $1/\lambda = 2\pi I_c L/\Phi_0 \to 0$] corresponds to the integrable sG model.

For zero external driving (and zero external field) the lowest energy configuration of phases corresponds to the uniform state $\varphi_j = 0$ (or $2\pi n$, in general).

When cooling in the presence of an external magnetic field, quanta of flux (fluxons), can be trapped in the array. When removing the external field (thus $\Phi^{\text{ext}} = 0$), fluxons remain trapped in the array. A fluxon in the array corresponds to a jump of $\pm 2\pi$ in the phases around the array (see Fig. 2). In the continuous limit, a fluxon corresponds to the sG soliton given by

$$\phi(x) = 4 \arctan\{\exp[x - X(t)]/l_0\} \,, \tag{7}$$

where $X(t)$ is the position of the soliton and l_0 stands for the soliton width, with $l_0 = \sqrt{\lambda}$ at low values of $1/\lambda$. sG solitons are invariant under continuous translations, and hence any finite force can move them. The sG model is suitable for modeling long JJs [6, 7, 18]; however, the parallel array is an intrinsically discrete system and is modeled by a discrete model (the FK model). In this system, the main consequence of considering the effect of the discretization is the loss of the continuous translational invariance property and hence the pinning of the fluxon. Thus, a non-zero force is needed to depin the fluxon (depinning force). An example of this effect can be observed in Fig. 2. To displace the fluxon site in the array, we need to go to a higher energy intermediate configuration, which is a saddle point of the phase's energy landscape. The energy difference between these configurations is usually known as the Peierls–Nabarro barrier [19] for the fluxon (from the dislocation theory).[2]

Thus, a fluxon has to overcome an energy barrier to go to the next plaquette. However, the dynamical properties of this process are not completely characterized by this barrier, but also by its shape, which is related to the critical forces, frequencies, relaxation times, etc. A way to accomplish this task is to identify the fluxon with a particle whose position is given by its center of mass. Following this idea, the collective coordinate method [20] allows for an analytical calculation of the profile of the barrier in the low pinning regime. Essentially, a functional form for the fluxon is assumed (usually that of the

---

[1] When writing (4) we assume only mesh self-inductances.

[2] Depending on the context a defect in the ground-state configuration is called a soliton, kink, dislocation or discommensuration. Since we are dealing with a superconducting system, the localized defect solution corresponds to a fluxon.

continuous limit). Then a perturbation method is used to treat the discreteness. The method works very well for low values of the discreteness parameter $(1/\lambda)$, but fails for the higher ones in which the width of the fluxon is of the order of the plaquette length.

To numerically compute the potential profile for the fluxon, we used the following procedure: first, we find the saddle-point configuration which corresponds to the fluxon on the top of the potential. Second, starting from this configuration we move the system to relax (using (6)) to the minimum-energy configuration. Such relaxation occurs by following the steepest direction on the energy landscape, given by the eigenvector associated with the only negative eigenvalue of the stability matrix of the configuration at the saddle point. During the relaxation we work out the energy and center of masses of the configuration, obtaining the potential profile $E(X_{CM})$:

$$X_{CM} = \frac{1}{2} + \frac{1}{2\pi} \sum_{j=1}^{N} j(\varphi_{j+1} - \varphi_j) \qquad (8)$$

and

$$E/E_J = \sum_j h_j (1 - \cos \varphi_j) + \frac{\lambda_j}{2} (\varphi_{j+1} - \varphi_j)^2 , \qquad (9)$$

where E_J is the characteristic Josephson energy of the junction, $E_J = \Phi_0 I_c / 2\pi$.

Finding the desired saddle-point configuration can be a very tough task. One possibility is to use intuition about this configuration in the small-λ limit. Another procedure is to first locate the minimum-energy configuration of a fluxon and then move the configuration slowly, fixing an appropriate phase and minimizing the rest of phases to the minimum of energy. The force needed to keep this configuration is calculated, and the process is iterated until a saddle point is reached where the force is zero and the linear stability analysis gives a negative

eigenvalue. In Fig. 3a we show the computed profile for the fluxon in a regular array with $\lambda = 0.25$.

3 Ratchet behavior

Different configurations of critical currents and cell areas result in different profiles for the fluxon potential. Using the concepts introduced in the previous section, we are ready to analyze the minimal conditions to achieve an effective potential for the fluxon in which mirror symmetry is absent, a fluxon ratchet potential. It is important to highlight that all interactions in the system are symmetric in the field variables (superconducting phases). Thus, the inversion symmetry breaking has to be geometrical, i.e. using the possibility of spatial variations of the array parameters. We have two sets of parameters available: plaquette self-inductances and junction critical currents.

We found two different simple possibilities for designing arrays which display fluxon ratchets potentials. The first case corresponds to the choice of junctions with two different critical currents and cells with two different areas (and thus two different values for the cell self-inductances). This conditions can be implemented in (5) by setting $\{I_{cj}\} = \{I_c, \alpha I_c, I_c, \alpha I_c, \ldots\}$, and $\{L_j\} = \{L, \beta L, L, \beta L, \ldots\}$, with α and β fixing the degree of asymmetry in our lattice. The second case corresponds to the choice of junctions with three different critical currents and equal-area cells. This conditions can be implemented in (5) by setting $\{I_{cj}\} = \{I_c, \tilde{\alpha} I_c, \tilde{\beta} I_c, I_c, \ldots\}$, and $\{L_j\} = \{L, L, \ldots\}$.

Using the method developed in the previous section, we calculated the fluxon energy profiles for four different array configurations. Figure 3 shows potential profiles for a set of the model parameters (λ, α, β) with $\lambda = 0.25$. In Fig. 3a $\alpha = 1.0$ and $\beta = 1.0$, which corresponds to a regular array. In Fig. 3b $\alpha = 0.5$ and $\beta = 1.0$ (different critical currents), and the energy profile shows a double-well structure symmetric with respect to the top of the wells. In Fig. 3c $\alpha = 1.0$ and $\beta = 0.5$ (different inductances), and the potential is symmetric with respect to the bottom of the wells. As expected, for other cases the potential profiles do not show inversion symmetry. The values $\alpha = 0.5$ and $\beta = 0.5$ (Fig. 3d) give a good approximation to the asymmetric sawtooth potential used in the literature [21] and form the desired fluxon ratchet potential.

We also computed, as a function of λ, the positive and negative values of the depinning current (the minimum current required to move the fluxon) and the PN barrier, E_{PN}, for the cases of the regular and ratchet ($\alpha = \beta = 0.5$) arrays (see Fig. 4). Assuming a sinusoidal profile for the fluxon potential, we expect to obtain a depinning current equal to $I_{PN}^{reg}/I_c = E_{PN}^{reg}/2E_J$ for the case of the regular array and $I_{PN}^{rat}/I_c = E_{PN}^{rat}/4E_J$ for the ratchet array, since the heights of the barriers are E_{PN} and the spatial periodicities are equal to 1 and 2 respectively.

The solid lines in the figure correspond to the two I_{PN} defined above. The depinning current values of the regular array adjust to the solid line as expected after Fig. 3a. For the case of the ratchet array the depinning current is different in the two directions, corresponding to different depinning currents in the plus (I_{dep}^+) and minus (I_{dep}^-) directions. We can see in the figure that for the case of our ratchet array I_{dep}^+
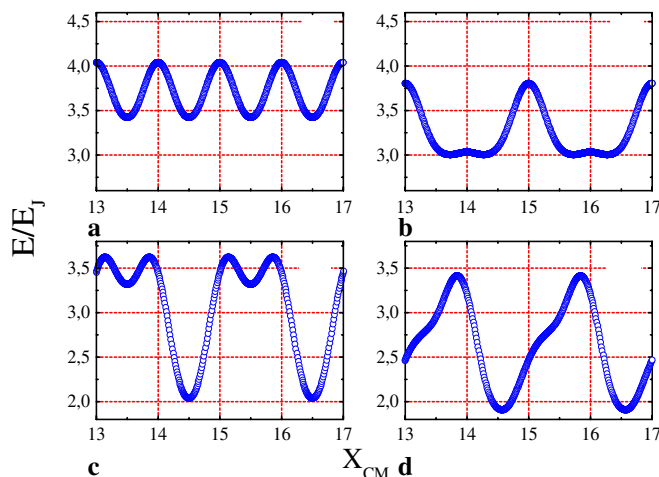

FIGURE 3 Energy profile $E(X_{CM})$ for different values of asymmetry parameters (α, β) and $\lambda = 0.25$. **a** $\alpha = \beta = 1.0$; regular array. **b** $\alpha = 0.5$, $\beta = 1.0$; different critical currents and same plaquette areas. **c** $\alpha = 1$, $\beta = 0.5$; same critical currents but different plaquette areas. **d** $\alpha = 0.5$, $\beta = 0.5$ gives a "ratchet-like" potential
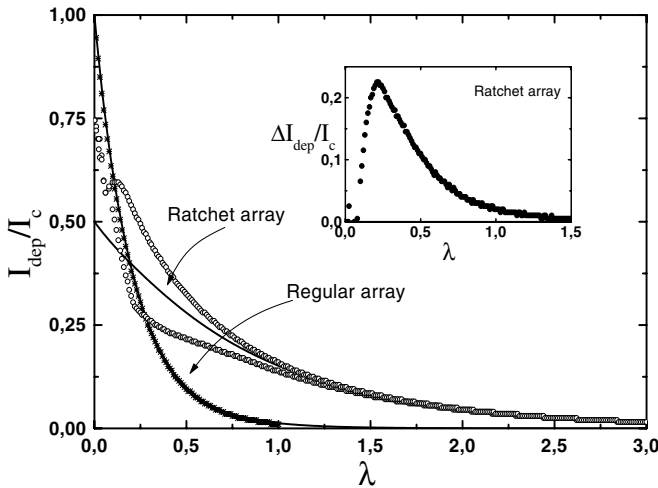
FIGURE 4 Fluxon depinning currents, I_{dep}, as a function of λ for the homogeneous and a ratchet ($\alpha = \beta = 0.5$) array. *Solid lines*: predictions from E_{PN} values (see text). *Symbols*: numerical computation of the depinning currents. *Inset*: difference (ΔI_{dep}) between the absolute values of the two depinning currents for the ratchet array

and I_{dep}^{-} are significantly different for values of λ between 0.1 and 0.9. In this region $I_{dep}^{-} > I_{dep}^{+}$. At large values of λ the depinning currents adjust to the expected value, pointing out an almost sinusoidal potential. The inset shows the difference ($\Delta I_{dep} = I_{dep}^{-} - I_{dep}^{+}$) between the values of the two depinning currents for the ratchet array. As we can see there exists a moderate range of values of λ for which an important ratchet behavior is expected. The maximum of these curves is obtained for $\lambda \sim 0.22$.

We also studied the case of an array with three different critical currents and all equal inductances. Computation of the potential profile in this device gives similar results to the other design, but now the spatial periodicity is equal to three sites of the array. Good parameter values for this case are $\tilde{\alpha} = 0.5$ and $\tilde{\beta} = 0.25$ at $\lambda = 0.25$.

We will study now the dynamical behavior of a fluxon in the asymmetric lattice. For all simulations, we take $N = 30$, $\lambda = 0.25$, $\alpha = 0.5$ and $\beta = 0.5$. We drive the system out of thermal equilibrium by applying an external ac bias current, $I(t)$. The normalized $I(\tau)/I_c$ term in (6) is then expressed as

$$I(\tau)/I_c = \frac{I_{ac}}{I_c} \sin \omega\tau + \xi(\tau) . \tag{10}$$

Here, $\xi(\tau)$ is white noise [$\langle \xi(\tau) \rangle = 0$ and $\langle \xi(\tau)\xi(\tau') \rangle = 2k_B T/E_J \delta(\tau - \tau')$] which, in the absence of other forces, brings the system to thermal equilibrium. Thus, the equations of motion take the form of a system of stochastic differential equations. We have solved them using a fourth-order Runge–Kutta method for the deterministic part and a third-order one for the stochastic part [22].

We will concentrate first on the deterministic ($T = 0$) dynamics. For a positive driving we find $I_{dep}^{+} \approx 0.28$ whereas for negative driving $I_{dep}^{-} \approx 0.495$ (for the symmetric case, $\alpha = 1.0$, $\beta = 1.0$ and $I_{dep} \approx 0.305$).

When applying ac currents we should observe an I–V curve (dc voltage versus current amplitude I_{ac}) showing rectification of the external current for current ampli-

tudes above the smallest of the depinning currents, and with a maximum efficiently for amplitudes close to the biggest one [2]. Figure 5 shows the I–V curves at $T = 0$ for three different values of the frequency, ω. The low-frequency response clearly resembles that found for a single particle [23]. As it was noted in one-particle simulations, voltage is quantized:

$$V/I_c R_s = \sum_{i=1}^{N} \langle \dot{\phi}_i \rangle = 2 \left(\frac{p}{q} \omega \right) , \tag{11}$$

p and q being integers. These voltage steps correspond to mode-locking attractors in which a fluxon moves $2p$ plaquettes in q periods of the driving force [10, 24]. For a finer resolution, the I–V curves appears to have a devil's staircase structure [23] (see inset of Fig. 5c).

Finally, we discuss the effect of thermal noise in the fluxon dynamics. At non-zero temperature the steps become rounder due to thermally activated jumps between the mode-locking attractors. At a high enough temperature (in the adiabatic limit) the whole step structure disappears and a smooth curve is found (see Fig. 6). In this limit we can fit the I–V curve with the solution of Magnasco [21] for a sawtooth ratchet potential. We found a good fit (see Fig. 6) for the asymmetry ratio, $\lambda_1/\lambda_2 = 0.56$, and energy barrier, $\Delta E/E_J = 1.6$, obtained from the computed energy profile (see Fig. 3d).
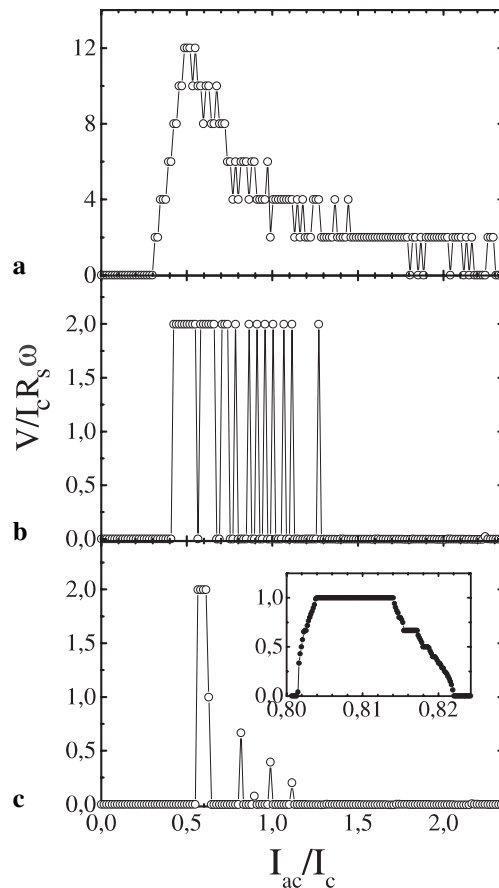

FIGURE 5 Voltage–current curves at $T = 0$ and with an ac current for different frequencies: **a** $\omega = 2\pi 0.0025$, **b** $\omega = 2\pi 0.0125$ and **c** $\omega = 2\pi 0.025$. $\lambda = 0.25$ and $\alpha = \beta = 0.5$
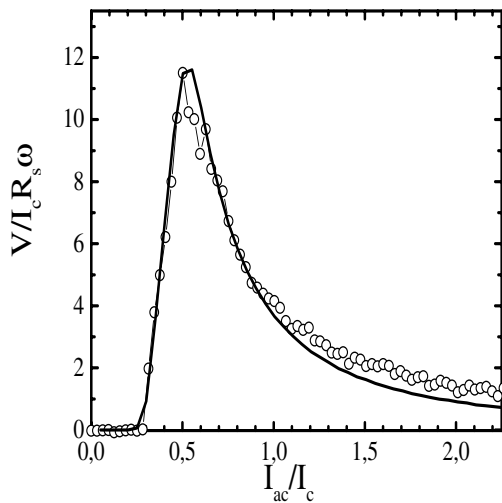
FIGURE 6 Voltage–current curves for an ac current at $T = 0.01$ and $\omega = 2\pi 0.0025$ (compare with Fig. 5a). *Thick line*: comparison with (3) of [21]
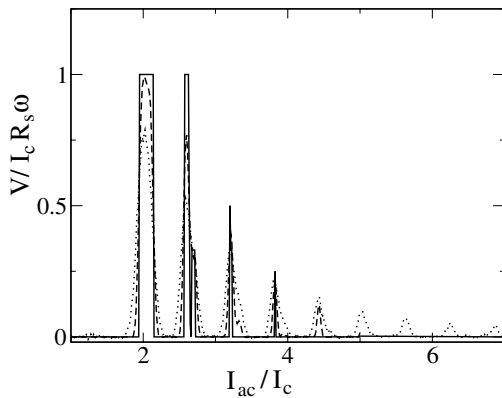

FIGURE 7 Voltage–current curves for an ac current for the three-junction model ($\lambda = 0.5$, $\tilde{\alpha} = 0.5$, $\tilde{\beta} = 0.25$) at $T = 0$ (*solid line*), $T = 0.005$ (*dashed line*) and $T = 0.025$ (*dotted line*) and $\omega = 2\pi 0.033$

At higher frequencies the I–V curves are more complex. Figure 7 show the curve for the three-junction model. At very low temperature the steps are stable with regard to thermal fluctuations and probably could be observed in real experiments. At higher temperatures, the first peaks became rounded and broadened, and surprisingly new peaks appeared at high currents which are absent in the deterministic curve. These thermal induced peaks are a consequence of jumps between very close stable and unstable pinned fixed points of the deterministic dynamics [25].

4   Experiments

To verify the theoretical predictions, we have designed and measured the four circular rings schematically shown in Fig. 8. Figure 9 illustrates the ratchet ring. Our purpose is to be able to compare the effects of the different array configurations on the fluxon properties. The rings are fabricated with an Nb–Al$_2$O$_x$–Nb tri-layer technology; we inject the current and measure the dc voltage across a junction. The measured arrays were not shunted by external resistors. Thus, a complete model for the junction current in this situation should include capacitive terms. This is not important
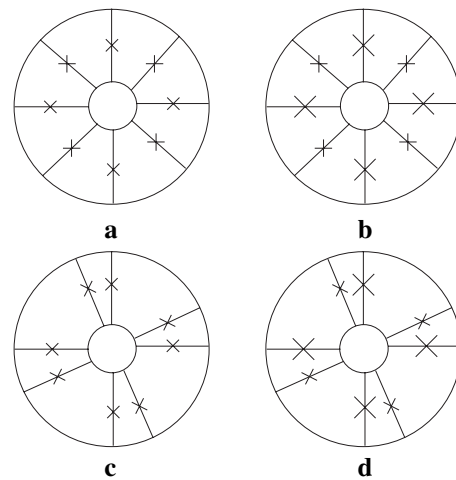

FIGURE 8 The four measured arrays: **a** regular ring ($\alpha = \beta = 1.0$), **b** ring with two alternating critical currents ($\alpha = 0.43$, $\beta = 1.0$), **c** ring with two alternating cell areas ($\alpha = 1.0$, $\beta = 0.53$) and **d** ratchet ring with alternating critical currents and cell areas ($\alpha = 0.43$, $\beta = 0.58$)
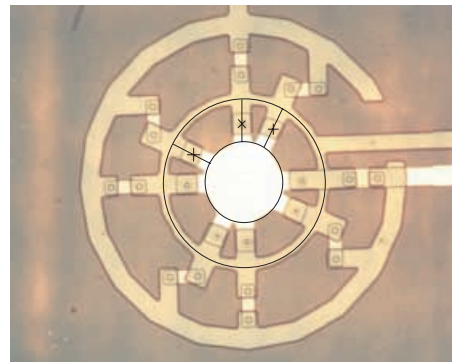

FIGURE 9 Picture of the ring array corresponding to a ratchet pinning potential with $\alpha \approx 0.5$ and $\beta \approx 0.5$

in this paper, since we have only probed depinning currents, which do not depend on the damping of the array. More details about the experimental setup can be found in [12]. It will be shown experimentally that only the circular ring in Fig. 8d has a ratchet pinning potential.

In Fig. 10 we show the typical measured I–V curves for the different rings shown in Fig. 8 biased by a dc current. Figure 10a is for the regular ring. As expected, the I–V curve is symmetric with respect to the applied current direction. In the superconducting state, the voltage remains at zero as the current is increased and stays at zero for currents below the depinning current. Beyond the depinning value, the voltage increases and some structure appears, as is shown. This structure is due to resonances and instabilities caused by the underdamped nature of the array. Figure 10b is a ring with alternating critical currents, and Fig. 10c a ring with alternating areas. In all the cases a single fluxon is trapped in the superconducting rings. In Fig. 10b and c we again see that the I–V curve is symmetric with respect to the current direction and that there is some voltage structure. Since for these three rings $I_{dep}^+ = I_{dep}^-$, we can infer that the kink travels on a symmetric pinning potential as theoretically expected.

Figure 10d shows an I–V curve for the ring with both alternating critical currents and areas. The I–V curve of this ring is qualitatively different from the other rings due to the
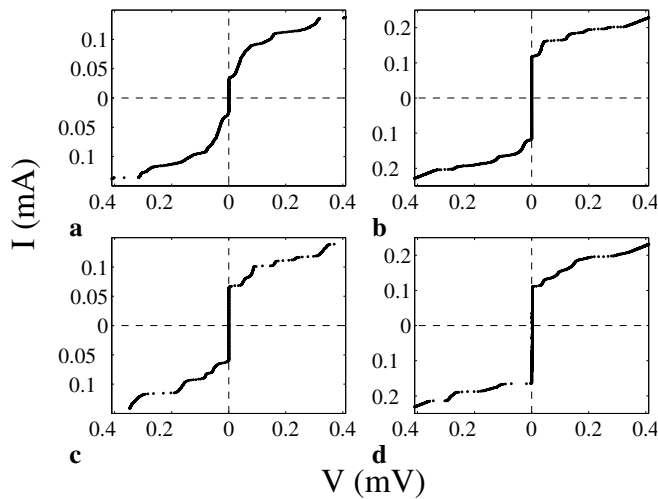
FIGURE 10 Current–voltage curves for the rings considered in Fig. 8 (**a** corresponds to Fig. 8a and so on). Rings **a**, **b**, and **c** have symmetric *I–V* curves as the current is swept in the positive and negative directions. The measurements correspond to one fluxon trapped in the array. Ring **d** is the ratchet ring, as can be seen from the difference in the depinning current in the positive and negative directions

ratchet nature of the pinning potential. We see that I_{dep} in the positive direction is $\sim 65\%$ of that in the negative direction. We also note a different voltage structure in the up and down directions. We will focus on I_{dep} measurements as a signature for ratchet behavior in our arrays.

In the experiments fluxons are trapped in the ring by cooling the sample in the presence of an external field. Once the array becomes superconducting, quanta of field, the fluxons, can be trapped in the array and remain trapped after remov-

ing the external field. Depending on the intensity of the field, a different number of fluxons, M, can be trapped. In a ring the critical current is only determined by the number of fluxons trapped, as can be inferred from (6) and the system boundary conditions. Then, it is an interesting issue to study the properties of the array as a function of the external field.

Figure 11a shows a measurement of the depinning current versus the applied flux for the regular ring shown in Fig. 8a. Each plateau in the figure represents a different number of fluxons trapped in the ring. This is a direct result of flux quantization: The ring only allows an integer number of flux quanta, even when slightly more or less flux is applied. Since $N = 8$ and this ring has a symmetric pinning potential, we expect $I_{\mathrm{dep}}^{+} = I_{\mathrm{dep}}^{-}$ (no ratchet effect) and a period of 8, as can be seen in the measurements. We also see that I_{dep} has a reflection symmetry at about $M = 4$.

When we alternate the critical currents in our ring, we expect the same qualitative features of I_{dep} as in the regular ring. Figure 11b shows a measurement of the depinning current versus applied flux for the ring shown in Fig. 8b which has two alternating critical currents. There are plateaus corresponding to different values of M just as in the regular ring; there is up–down symmetry and periodicity with $M = 8$ as expected and reflection symmetry at about $M = 4$.

If we make all the critical currents constant and vary only the cell area, as in Fig. 8c, then we alternate the values of λ, but the pinning potential remains symmetric. The result of measuring I_{dep} is shown in Fig. 11c. As expected the data is symmetric with respect to the current direction, so kinks are not traveling in a ratchet pinning potential. However, unlike in the previous rings, I_{dep} is no longer periodic with $M = 8$. Such an effect was predicted in [12], where it was shown
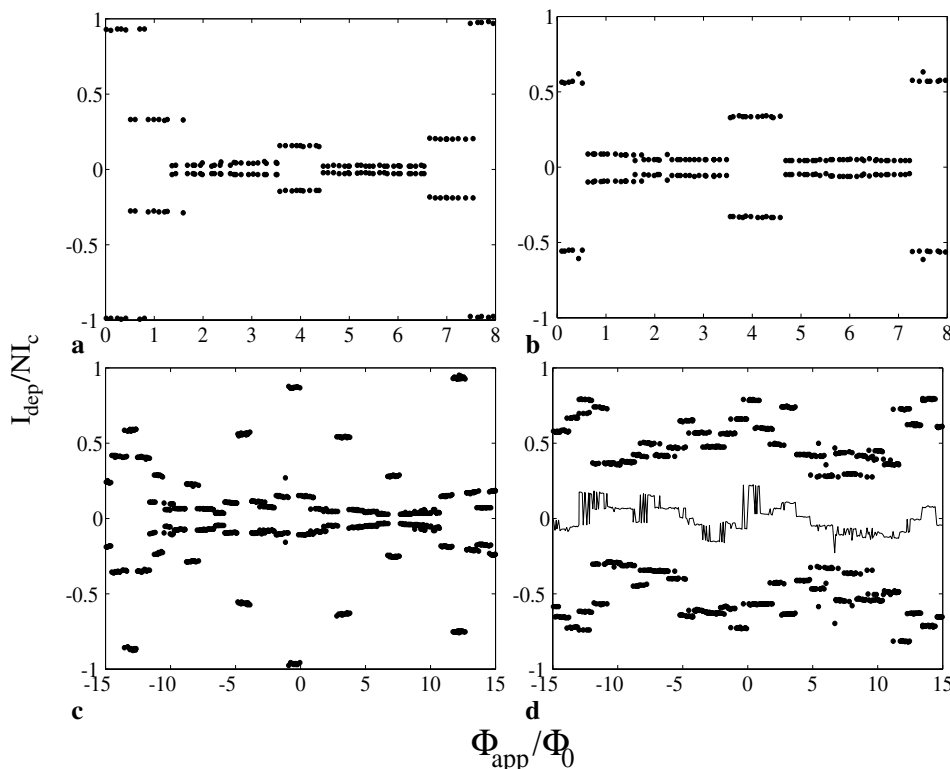

FIGURE 11 Measured critical currents versus the applied flux for the four types of rings. The measurements was made at **a** $T = 8.8\,\mathrm{K}$ with $\lambda \approx 0.9$; **b** $T = 9\,\mathrm{K}$ with $\lambda \approx 0.9$; **c** $T = 9\,\mathrm{K}$ with $\lambda_{\mathrm{l}} \approx 0.7$ and $\lambda_{\mathrm{s}} \approx 1.3$; and **d** $T = 8.8\,\mathrm{K}$ with $\lambda_{\mathrm{l}} \approx 0.3$ and $\lambda_{\mathrm{s}} \approx 0.6$. In this last case, the *line* varying about $I_{\mathrm{dep}} = 0$ is the difference between I_{dep}^{+} and I_{dep}^{-}

that the period depends on the ratio of the inductances. For our geometry $L_1/L_2 \approx 1.8$ or $9/5$, which implies a period of 56. However, in any physical array the inductance ratio is rarely going to be exactly a ratio of small numbers. Just on physical grounds we expect a very large period, if any, in the experiments. In Fig. 11c the depinning current we measured from $M = -15$ to $M = 15$ is shown, and though there is some apparent self-similarity in the data, it is not periodic. Though there is no period, we can still prepare our ring systematically with $M = 1, 2, 3$, etc., by counting the plateaus. But instead of $M = 1$ and $M = 1 + N$ yielding the same dynamical system as in the regular ring, they are now distinguishable.

When we alternate both the critical current and the cell inductances as in Fig. 8d, it is possible to form a ratchet pinning potential (see Fig. 3d). Figure 11d shows an experiment on such a ring. Since the period depends on the inductance ratio, we experimentally expect a very long period. This is borne out by the data, as there is no sign of a period in the range from $M = -15$ to 15. We also expect that $I_{dep}^+ \neq I_{dep}^-$, since the kink is traveling in a ratchet pinning potential. The line shown in the center of the figure varying about $I_{dep} = 0$ is the difference between the I_{dep}^+ and I_{dep}^-. Clearly, the force to move kinks in one direction is different than the force to move it in the opposite direction. The magnitude and direction of this ratchet effect depends on the number of kinks in the system.

5   Conclusion

The study of fluxons in Josephson-junction parallel arrays provides an excellent opportunity to check the predictions of the theory about directional motion of particles in ratchet potentials. We have shown that quite simple designs on a Josephson-junction parallel array produce controllable potential profiles. The experiments nicely fit the main predictions of the theory.

The results reviewed here open the possibility for further studies. For instance, experiments under ac currents are still to be performed. In addition, a finite density of fluxons can easily be introduced in the array, and then genuine collective effects could be observed. In this case, fluxon–fluxon or fluxon–phonon interactions will play an important role.

Finally, the feasibility of going into the quantum regime (by reducing the system sizes and the temperature), opens the possibility of studying the ratchet effect in a quantum macroscopic object.

REFERENCES

1 P. Reimann: Phys. Rep. **361**, 57 (2002) and references therein; a recent popular article about ratchets is R.D. Astumian: Sci. Am. July, 57 (2001)
2 R.D. Astumian: Science **276**, 917 (1997)
3 F. Jülicher, A. Ajdari, J. Prost: Rev. Mod. Phys. **69**, 1269 (1997)
4 M. Porto, M. Urbakh, M. Klafter: Phys. Rev. Lett. **84**, 6058 (2000)
5 I. Zapata, R. Bartussek, F. Sols, P. Hänggi: Phys. Rev. Lett. **77**, 2292 (1996)
6 G. Carapella: Phys. Rev. B **63**, 054 515 (2001); G. Carapella, G. Costabile: Phys. Rev. Lett. **87**, 077 002 (2001)
7 S. Weiss, D. Koelle, J. Müller, R. Gross, K. Barthel: Europhys. Lett. **51**, 499 (2000); E. Goldobin, A. Sterck, D. Koelle: Phys. Rev. E **63**, 031 111 (2001)
8 C.S. Lee, B. Janko, I. Derényi, A.L. Barabasi: Nature **400**, 337 (1999)
9 J.F. Waunbaugh, C. Reichardt, C.J. Olson, F. Marchesoni, F. Nori: Phys. Rev. Lett. **83**, 5106 (1999)
10 L.M. Floría, J.J. Mazo: Adv. Phys. **45**, 505 (1996)
11 F. Falo, P.J. Martínez, J.J. Mazo, S. Cilla: Europhys. Lett. **45**, 700 (1999)
12 E. Trías, J.J. Mazo, F. Falo, T.P. Orlando: Phys. Rev. E **61**, 2257 (2000)
13 T.P. Orlando, K.A. Delin: *Foundations of Applied Superconductivity* (Addison-Wesley, New York 1991)
14 S. Watanabe, S.H. Strogatz: Physica D **74**, 197 (1994)
15 K. Nakajima, Y. Onodera: J. Appl. Phys. **49**, 2958 (1978); A.V. Ustinov, M. Cirillo, B.A. Malomed: Phys. Rev. B **47**, 8357 (1993); S. Watanabe, H.S.J. van der Zant, S.H. Strogatz, T.P. Orlando: Physica D **97**, 429 (1996)
16 R.B. Griffiths: In *Fundamental Problems in Statistical Mechanics VII*, ed. by H. Van Beijeren (North Holland, Amsterdam 1990)
17 O.M. Braun, Y.S. Kivshar: Phys. Rep. **306**, 1 (1998)
18 D.W. McLaughlin, A.C. Scott: Phys. Rev. A **18**, 1652 (1978)
19 F.R.N. Nabarro: *Theory of Crystal Dislocation* (Dover, New York 1967); M. Peyrard, M.D. Kruskal: Physica D **14**, 88 (1984)
20 C.R. Willis, M. El-Batanouny, P. Stancioff: Phys. Rev. B **33**, 1904 (1986); P.J. Martínez, F. Falo, J.J. Mazo, L.M. Floria, A. Sanchez: Phys. Rev. B **56**, 87 (1997); A. Sánchez, A.R. Bishop: SIAM Rev. **40**, 579 (1998)
21 M.O. Magnasco: Phys. Rev. Lett. **71**, 1477 (1993)
22 H.S. Greenside, E. Helfand: Bell Syst. Tech. J. **60**, 1927 (1981)
23 R. Bartussek, P. Hänggi, J.G. Kissner: Europhys. Lett. 28, 459 (1994); P. Hänggi, R. Bartussek: In *Nonlinear Physics of Complex Systems, Lectures Notes in Physics, Vol 476* (Springer, Berlin, Heidelberg 1996) pp. 294–308
24 L.M. Floría, F. Falo: Phys. Rev. Lett. **68**, 2713 (1992)
25 S. Cilla: Ph.D. dissertation, Universidad de Zaragoza (2000)